Structure of eigenfunctions in terms of classical trajectories in an SU(3) schematic shell model

P. Leboeuf
*Division de Physique Théorique, Institut de Physique Nucléaire, 91406 Orsay CEDEX, France**
and Departamento de Física, Comisión Nacional de Energía Atómica, Av. Libertador 8250, 1429 Buenos Aires, Argentina

M. Saraceno
Departamento de Física, Comisión Nacional de Energía Atómica, Av. Libertador 8250, 1429 Buenos Aires, Argentina
(Received 10 October 1989)

The Husimi distribution for the eigenstates of a classically nonintegrable two-dimensional system with mixed phase space was calculated in order to analyze its structure in terms of classical trajectories. Besides eigenfunctions concentrated on invariant tori or with support on chaotic regions of phase space, we also found others that combine different classical invariant sets (like a stable and an unstable periodic orbit) and families of eigenstates scarred by classically unstable periodic orbits.

I. INTRODUCTION

A basic goal of semiclassical quantum mechanics is to provide a connection between classical trajectories and eigenvalues and eigenfunctions of a given system. In this paper we are concerned with a particular aspect of this quantal-classical correspondence: the interpretation of the structure of *individual* eigenfunctions of Hamiltonian systems in terms of classical trajectories when the system has a *mixed* phase-space structure, i.e., a mixture of regular and chaotic motion in the classical limit.

Since the semiclassical theory of such systems is far from being completed, our purpose here is to present numerical results illustrating how different trajectories combine in order to build up a given eigenfunction. We do not pretend to recover the eigenfunctions or the eigenvalues starting from classical mechanics but just the opposite way: given a certain eigenfunction, we want to identify classical patterns on it. Doing so, we hope to shed some light on the kind of problems we are facing from the theoretical point of view.

In order to compare directly the classical and the quantum solutions we must formulate both theories in terms of a unifying mathematical formalism. A particularly convenient representation of quantum mechanics is provided by the coherent states in which to the squared modulus of an (arbitrary) wave function is associated a positive definite phase-space distribution (sometimes called the Husimi distribution[1]). An important property of this distribution crucial to our purposes is that in the semiclassical limit the Husimi distribution associated to an eigenfunction of a Hamiltonian system peaks *smoothly* on the classical trajectories;[2,3] the typical singularities and nonanalyticities of the semiclassical limit, although of great interest,[4,5] are eliminated in the Husimi representation.

From the correspondence principle we expect, in the semiclassical limit, that a phase-space Husimi distribution associated to a certain eigenfunction approaches some classical stationary distribution localized on the corresponding energy shell. For integrable systems, we know that the eigenfunctions are peaked on the quantized invariant torus. On the contrary, in the case of strongly chaotic motion where no invariant tori exist we expect a spreading of the eigenfunctions over the entire energy shell. In fact, some theorems prove[6,7] that this set is the invariant set supporting almost all eigenfunctions of ergodic systems in the semiclassical limit. However, several recent studies[8–11] show that many eigenfunctions of these systems are far from being "uniform" distributions over the energy shell but present simple regular patterns that can, in general, be interpreted in terms of periodic orbits. Finally, in the case of mixed systems we get an even more complicated classical phase-space structure, where the minimal invariant sets are, apart from the energy shell as a whole, the (bounded) chaotic regions, tori, cantori, and periodic orbits.[12] Very little is known about the structure of individual eigenstates of such systems and their connection to the classical invariant sets, a point we want to address.

The results we are going to present were obtained in a many-body system related to nuclear physics, a schematic shell model with SU(3) symmetry whose classical counterpart is represented by a two degrees of freedom conservative Hamiltonian. Although the model is far from being the simplest system having a mixed phase space (for instance, it has no energy scaling and it is not defined as a map), it has the important property that its Hilbert space is compact, and therefore there are no numerical errors introduced by a truncation of the basis. Moreover, it provides an example of how models not belonging to the usual Weyl group can also be treated in a simple way.[13]

II. THE SU(3) MODEL

A. Quantum description

The SU(3) model is a three-level schematic nuclear shell model.[14,15] It is defined by N interacting fermions

 ©1990 The American Physical Society

that can occupy three different single particle levels (shells): 0, 1, and 2 for the ground, first, and second excited states with energies ε_i. Each shell is N degenerate so that fermions are labeled by an index $m=1,\ldots,N$ (see Refs. 16, 17, and 13 for more details of quantum and classical aspects of the model).

The Hamiltonian of the system can be written in the following way:

$$H=H_0+V\ ,$$
$$H=\sum_{i=0}^{2}\varepsilon_i G_{ii}+\frac{1}{2}\sum_{i\neq j=0}^{2}v_{ij}G_{ij}^2\ , \tag{2.1}$$

where

$$G_{ij}=\sum_{m=1}^{N}a_{im}^{\dagger}a_{jm};\quad G_{ij}^{+}=G_{ji},\quad i,j=0,1,2 \tag{2.2}$$

are "collective" operators completely symmetric under the interchange of two fermions obeying a U(3) algebra.[14] However, as is explained below, the conservation of the total number of particles implies that we can eliminate one of the generators, resulting in an SU(3) algebra. The $(a_{im}^{\dagger},a_{im})$ are the usual fermionic operators obeying anticommutation relations which create and/or annihilate the fermion m of the i shell and v_{ij} are interaction parameters.

We are going to work on the representation of the group for which all the particles are in the lowest shell 0 in the noninteracting ground state (the $[N\,0\,0]$ representation of the group). Because the interaction conserves the total number N of particles, a basis of this representation can be labeled by the occupation numbers n_i of only *two* of the three shells [we choose shells 1 and 2, the occupation numbers of the lowest shell 0 being given by Eq. (2.4) below],

$$|n_1n_2\rangle=\left[\frac{N!n_1!n_2!}{(N-n_1-n_2)!}\right]^{1/2}G_{10}^{n_1}G_{20}^{n_2}|0\rangle \tag{2.3}$$

where $|0\rangle$ is the vacuum state for which all the particles are in the lowest shell 0.

These states are eigenstates of the particle number operators G_{11} and G_{22} with eigenvalues n_1 and n_2, respectively. Due to conservation of N, the n_i satisfy the equation

$$n_0=N-n_1-n_2 \tag{2.4}$$

with

$$0\leq n_1+n_2\leq N \tag{2.5}$$

and it is then clear that the states (2.3) are also eigenstates of G_{00} and therefore of H_0. We use the operator version of (2.4),

$$G_{00}=N-G_{11}-G_{22}\ , \tag{2.6}$$

to eliminate in (2.1) the occupation number G_{00} of the lowest shell; all the results from now on are going to be expressed only in terms of the variables labeling the shells 1 and 2.

The second term on the right-hand side of Eq. (2.1) represents a two-body interaction that moves *pairs* of particles between levels. Due to the fact that the interaction conserves the oddness or evenness of the occupation numbers, when written in the basis (2.3), the Hamiltonian of the system splits into four blocks determined by the parity of n_1 and n_2. The dimension of the different parity blocks of H for N even or odd are given in Table I. In the numerical calculations presented in Sec. IV B we have used N even and computed eigenstates of the $(+,+)$ multiplet, to which the ground state of the system belongs.

B. The classical limit

The classical limit of the SU(3) model is obtained when the total number of particles N goes to infinity.[16,17,13] In particular, in Ref. 17 Meredith, Koonin, and Zirnbauer have compared, considering the classical underlying phase-space structure, the spectral fluctuations and overlap probability distributions of the eigenstates of the system with Gaussian orthogonal ensemble (GOE) predictions.

Using the appropriate coherent states for the $[N\,0\,0]$ representation, which are parametrized by two complex parameters z_1 and z_2,

$$|z_1z_2\rangle=\exp(\bar{z}_1G_{10}+\bar{z}_2G_{20})|0\rangle\ , \tag{2.7}$$

and making a (noncanonical) change of variables $(z_i,\bar{z}_i)\rightarrow(I_i,\theta_i)$ to the action-angle variables of the unperturbed Hamiltonian H_0,

$$z_i=\left[\frac{I_i}{1-I_1-I_2}\right]^{1/2}e^{i\theta_i},\quad i=1,2\ , \tag{2.8}$$

the classical limit of Hamiltonian (2.1) is given by

$$\mathcal{H}(I,\theta)=\mathcal{H}_0(I)+\chi\mathcal{V}(I,\theta)\ ,$$
$$\mathcal{H}(I,\theta)=-1+I_1+2I_2$$
$$+\chi[(1-I_1-I_2)(I_1\cos2\theta_1+I_2\cos2\theta_2)$$
$$+I_1I_2\cos2(\theta_2-\theta_1)]\ , \tag{2.9}$$

TABLE I. Dimension of the different parity multiplets of H.

	$(+,+)$	$(+,-)$	$(-,+)$	$(-,-)$
N even	$\frac{(N+2)(N+4)}{8}$	$\frac{N(N+2)}{8}$	$\frac{N(N+2)}{8}$	$\frac{N(N+2)}{8}$
N odd	$\frac{(N+1)(N+3)}{8}$	$\frac{(N+1)(N+3)}{8}$	$\frac{(N+1)(N+3)}{8}$	$\frac{(N-1)(N+1)}{8}$

which is a two degrees of freedom stationary Hamiltonian. In deriving Eq. (2.9) we have chosen the parameters

$$\varepsilon_0=-1,\quad \varepsilon_1=0,\quad \varepsilon_2=1$$
$$v_{ij}=v_{ji}=v,\quad \forall i\neq j \tag{2.10}$$

in (2.1), we have introduced the new interaction parameter χ via

$$\chi=(N-1)v \tag{2.11}$$

and we have normalized the Hamiltonian $\mathcal{H}(I,\theta)$ by the total number of particles N [with the choice (2.10) for the single-particle energies, the energy and interaction parameter χ correspond to dimensionless quantities]. Through the canonical transformation

$$q_i=\sqrt{2I_i}\cos\theta_i,\quad p_i=\sqrt{2I_i}\sin\theta_i,\quad i=1,2 \tag{2.12}$$

Eq. (2.9) can be written in the usual (p,q) coordinates; we then get a Hamiltonian which has not the kinetic plus potential form and containing terms of fourth order in p.[16]

Putting $\chi=0$, Eq. (2.9) reduces to two uncoupled harmonic oscillators written in action-angle variables, with frequencies $w_1=1$ and $w_2=2$. The action variables I_1 and I_2, therefore, represent the classical continuous version of the normalized occupation numbers n_1/N and n_2/N, respectively, defined as

$$I_i=\frac{1}{N}\frac{\langle z_1z_2|G_{ii}|z_1z_2\rangle}{\langle z_1z_2|z_1z_2\rangle}\ . \tag{2.13}$$

The term in χ in the classical Hamiltonian (2.9) is the classical analog of the two-body interaction term of (2.1), and provides an interaction between the oscillators. There is, however, an important difference between these oscillators and the usual Weyl group oscillators due to the fact that we have now an upper bound limit to the total number of particles that can occupy the shells 2 and 3. The classical statement of this finite-size effect is obtained taking the coherent-state representation of (2.6) and definition (2.13) to obtain

$$I_0+I_1+I_2=1 \tag{2.14}$$

that imposes the following restriction to the classical actions [cf. (2.5)]:

$$0\leq I_1+I_2\leq 1\ . \tag{2.15}$$

This equation states that the classical phase space obtained is a compact space, a fact related to the finite size of the irreducible representations of the SU(3) group.

The dynamics of the system in this limit is provided by the usual Hamilton equations (they correspond to the time-dependent Hartree-Fock approximation of the quantum fermion dynamics)

$$\dot\theta_i=\frac{\partial\mathcal{H}}{\partial I_i}\ , \tag{2.16}$$

$$\dot I_i=-\frac{\partial\mathcal{H}}{\partial\theta_i}\ , \tag{2.17}$$

or, using (2.9),

$$\begin{aligned}
\dot\theta_1&=1+\chi\cos2\theta_1-2\chi I_1\cos2\theta_1\\
&\quad-\chi I_2[\cos2\theta_2+\cos2\theta_1-\cos2(\theta_2-\theta_1)]\ ,\\
\dot\theta_2&=2+\chi\cos2\theta_2-2\chi I_2\cos2\theta_2\\
&\quad-\chi I_1[\cos2\theta_2+\cos2\theta_1-\cos2(\theta_2-\theta_1)]\ ,\\
\dot I_1&=2\chi(1-I_1-I_2)I_1\sin2\theta_1-2\chi I_1I_2\sin2(\theta_2-\theta_1)\ ,\\
\dot I_2&=2\chi(1-I_1-I_2)I_2\sin2\theta_2+2\chi I_1I_2\sin2(\theta_2-\theta_1)\ .
\end{aligned} \tag{2.18}$$

From the last two of Eqs. (2.18) it can be shown that the total number of particles is conserved by the equations of motion, i.e., $\dot I_1+\dot I_2=-\dot I_0$, and therefore Eqs. (2.14) and (2.15) are preserved by the dynamics.

The Hamiltonian (2.9) has two discrete symmetries, corresponding to the quantum splitting in four parity multiplets. These are

$$\begin{aligned}
&(\theta_1,\theta_2)\rightarrow-(\theta_1,\theta_2)\ ,\\
&(\theta_1,\theta_2)\rightarrow(\pi-\theta_1,\pi-\theta_2)\ .
\end{aligned} \tag{2.19}$$

Therefore the trajectories will always appear as single, double, or quadruple symmetry partners depending on whether none, one, or both symmetries (2.19) are broken.

We have thus obtained for the classical limit of the SU(3) model a two degrees of freedom Hamiltonian defined on a compact four-dimensional phase space with a dynamics provided by Eqs. (2.18). The only constant of the motion is the energy and therefore the Hamiltonian flow will be globally nonintegrable. There are, however, for any χ, as we will see, regions of phase space where most trajectories lie on invariant tori. As the energy changes, these are mixed with other regions where chaotic motion prevails.

The model has an extremely rich classical structure. There are many stationary points (both stable and unstable) which branch out as the interaction parameter χ grows. It cannot be represented as a kinetic plus potential energy Hamiltonian and thus phase-space methods are imperative. Moreover, only a finite range of energies is allowed, reflecting the fact that the phase space is compact.

As our objective is a comparison of the eigenfunctions of the system with classical structures, we now proceed to a more detailed analysis of the associated classical phase space.

III. CLASSICAL PHASE-SPACE STRUCTURE

In order to begin with an analysis of the different regions of phase space, let us calculate the location and stability of the stationary points of (2.9). For that purpose, we must solve the set of equations

$$\nabla\mathcal{H}=0\ . \tag{3.1}$$

This represents a system of four nonlinear coupled equations [cf. (2.18)]. We were able to find analytically 13 different stationary points of $\mathcal{H}$ and determine their stability. One more solution was found numerically.

Not all these solutions exist for all values of χ. In Table II we summarize the energies, coordinates, normal

TABLE II. Energy, coordinates, normal mode frequencies, and range of validity as a function of the interaction parameter χ of the 14 stationary points of the classical Hamiltonian (2.9), labeled from *A* to *N*. The hyphen appearing in some values of the angles indicates that any value of that coordinate is allowed. Point *G* was obtained numerically. The ordering employed corresponds to increasing energy (from *A* to *N*) when the value 10 is adopted for the interaction parameter (see Fig. 1).

Point	E	I_1	I_2	θ_1	θ_2	ω_1^2	ω_2^2	Validity
A	$\frac{-(\chi+1)^2}{4\chi}$	$\frac{\chi-1}{2\chi}$	0	$\pi/2$		$2(\chi^2-1)$	$\frac{1}{4}(\chi+1)(\chi+5)$	$\lvert\chi\rvert\geq 1$
B	$\frac{-(\chi^2+4)}{4\chi}$	0	$\frac{\chi-2}{2\chi}$		$\pi/2$	$\left\lvert\frac{\chi^2}{4}-4\right\rvert$	$2(\chi^2-4)$	$\lvert\chi\rvert\geq 2$
C	$\frac{-(\chi+1)^2}{5\chi}$	$\frac{\chi-4}{5\chi}$	$\frac{\chi+1}{5\chi}$	$\pi/2$	$\pi/2$	$\frac{4}{25}(\chi+1)[7\chi-13+(64\chi^2-152\chi-191)^{1/2}]$	$\frac{4}{25}(\chi+1)[7\chi-13+(64\chi^2-152\chi-191)^{1/2}]$	$-1\geq\chi\geq 4$
D	$\frac{-(\chi-1)^2}{4\chi}$	$\frac{\chi+1}{2\chi}$	$\frac{\chi-1}{2\chi}$		$\theta_1+\pi/2$	$2(\chi^2-1)$	$\frac{1}{4}(1-\chi)(5-\chi)$	$\lvert\chi\rvert\geq 1$
E	$\frac{-(\chi^2-5)}{5\chi}$	$\frac{3}{5}$	$\frac{\chi+5}{5\chi}$	$\pi/2$	0	$4(\chi^2/25-6\chi/5-1)$ $+4(16\chi^4/625-12\chi^3/125-19\chi^2/25+12\chi/5+1)^{1/2}$	$4(\chi^2/25-6\chi/5-1)$ $-4(16\chi^4/625-12\chi^3/125-19\chi^2/25+12\chi/5+1)^{1/2}$	$\lvert\chi\rvert\geq 5$
F	$\frac{-(\chi-1)^2}{5\chi}$	$\frac{\chi+4}{5\chi}$	$\frac{3(\chi-1)}{5\chi}$	0	$\pi/2$	$+\frac{4}{25}\{(\chi^2-32\chi+6)+$ $[(\chi^2-32\chi+6)^2+15(\chi-1)^2(\chi+4)(\chi-6)]^{1/2}\}$	$-\frac{4}{25}\{[(\chi^2-32\chi+6)-$ $[(\chi^2-32\chi+6)^2+15(\chi-1)^2(\chi+4)(\chi-6)]^{1/2}\}$	$-4\geq\chi\geq 1$
G								$\chi\geq 6$
H	-1	0	0			$(1-\chi^2)$	$(4-\chi^2)$	$\forall\chi$
I	0	1	0			$(1-\chi^2)$	$(1-\chi^2)$	$\forall\chi$
J	$+1$	0	1			$(1-\chi^2)$	$(4-\chi^2)$	$\forall\chi$
K	$\frac{(\chi-1)^2}{4\chi}$	$\frac{\chi+1}{2\chi}$	0	0		$2(\chi^2-1)$	$\frac{3}{4}(1-\chi)(3+\chi)$	$\lvert\chi\rvert\geq 1$
L	$\frac{\chi^2+4}{4\chi}$	0	$\frac{\chi+2}{2\chi}$		0	$\frac{-3}{4}\chi^2$	$2(\chi^2-4)$	$\lvert\chi\rvert\geq 2$
M	$\frac{(\chi+1)^2}{4\chi}$	$\frac{\chi-1}{2\chi}$	$\frac{\chi+1}{2\chi}$		$\theta_2=\theta_1$	$2(\chi^2-1)$	$\frac{3}{4}(1+\chi)(3-\chi)$	$\lvert\chi\rvert\geq 1$
N	$\frac{\chi}{3}+\frac{1}{\chi}$	$\frac{1}{3}$	$\frac{1}{\chi}+\frac{1}{3}$	0	0	$\frac{4}{3}[\chi^2-3+(3\chi^2+9)^{1/2}]$	$\frac{4}{3}[\chi^2-3-(3\chi^2+9)^{1/2}]$	$\lvert\chi\rvert\geq 3$

mode frequencies, and the range in χ where the solutions exist. The fourteen points are labeled from A to N. For $\chi=10$ (the value of the interaction parameter we will use for the numerical calculations), they are ordered by increasing energy. The sign of ω_i^2 determines the stability of each solution: both positives, stable; one negative, unstable along one normal direction; both negatives, unstable along both directions. The hyphen appearing in the value of the angle of certain stationary points means that any value of it is allowed.

Figure 1 shows the energy of these stationary points as a function of χ, for $\chi \geq 0$. The continuous lines represent stable stationary points, while dotted lines are unstable stationary points. We have only analyzed the $\chi>0$ case because for the special parameters chosen in (2.10) the solutions for $\chi<0$ can be deduced by simply changing the sign of the energy. In this sense it should be noticed that our convention for the sign of χ differs from that of Ref. 16, the difference resulting in an opposite sign for the energies.

As the interaction parameter χ grows, the phase-space structure evolves through branchings of the stationary points from a relatively simple situation with three stable stationary points for $\chi \leq 1$ to 14 stationary points for $\chi=10$, five of which are stable and nine unstable. The branching points have been indicated by heavy dots. At these values of χ there is usually a change in the symmetry of the stationary points. Thus, for example, for $\chi<1$ the upper stable branch has both symmetries (2.19). Between $\chi=2$ and 3 it has only one and therefore it represents two degenerate stable points. For $\chi>3$ all symmetries have been broken and there is a fourfold degeneracy. A similar analysis can be done for the other branches.

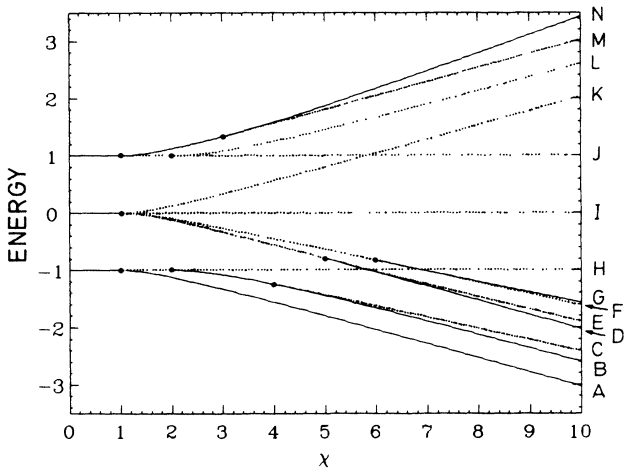

FIG. 1. Energy of the stationary points of the classical Hamiltonian as a function of the interacation parameter χ. The solid lines represent stable stationary points, while dotted lines the unstable stationary points. Labels $A-N$ for $\chi=10$ correspond to the labeling of Fig. 1. The branching points have been indicated by heavy dots.

Near each stable stationary point the Hamiltonian can be approximated by two uncoupled harmonic oscillators. We then expect to find a regular region in the neighborhood of each of them. As we move away from these points, we can think of the anharmonicities as a perturbation to this approximation, the energy measured from the stable point being the perturbation Kol'mogorov-Arnol'd-Moser (KAM) parameter. We have checked numerically the existence of these regular regions, and established the fact that they occupy most of the phase space associated to the well up to the energy of the nearest unstable point, after which a large portion of the tori are destroyed.

On the other hand, far from these stable points, for example, near $E=0$ for $\chi=10$, we have checked that the phase space is almost covered by chaotic trajectories.

To illustrate these facts, in Fig. 2 we show two Poincaré sections for several trajectories at $\chi=10$ lying (in energy) close to the upper stable stationary point N (that has $E=3.4\bar{3}$). The sections were made through the plane $I_2=0.4$ and displayed in the polar variables (I_1,θ_1). The circles correspond to the maximum allowed value for I_1, i.e., $I_1=1-I_2=0.6$ [cf. (2.15)]. The energy of the nearest unstable point is $E=3.025$ (point M of Fig. 1). Part (a) of the figure shows several trajectories with energy $E=3.1568$, intermediate between the stable and unstable points: they all lie on invariant tori; it is also clear the appearance of higher-order tori (the chaotic regions are too small to be visible). Part (b) shows the same section but for trajectories with $E=2.8946$, below 3.025: although we still find some trajectories lying on invariant tori, a large portion of them have been destroyed and now chaotic motion occupies a large portion of the available phase space.

Besides the stationary points, periodic orbits are also very important. For nonintegrable systems, they form one-parameter families isolated in the energy shell which can branch and bifurcate in very complicated trees.[18] We have not attempted such an exhaustive numerical study for the SU(3) model but instead we have concentrated on those families which exist because of the symmetries of the Hamiltonian and which are very simple. To find them we notice that the Hamiltonian (2.9) has three invariant planes defined by

$$I_1=0, \quad I_2=0, \text{ and } I_1+I_2=1 . \tag{3.2}$$

In fact, it is easy to check from the last two of equations

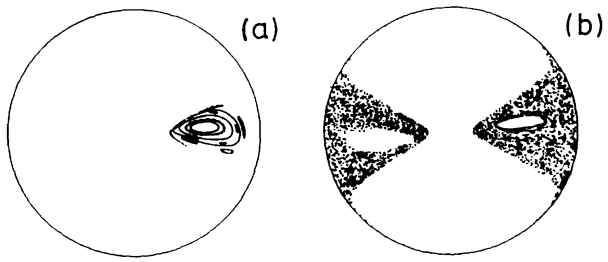

FIG. 2. Classical Poincaré sections for several trajectories at $\chi=10$ located close to the maximum stable stationary point N; (a) Trajectories whose energy is above the unstable stationary point M and (b) for an energy below that of point M.

(2.18) that

$$I_i=0 \Rightarrow \dot{I}_i=0, \quad i=1,2 \tag{3.3}$$

$$I_1+I_2=1 \Rightarrow \dot{I}_1+\dot{I}_2=0 \ . \tag{3.4}$$

In these special planes the motion has only one degree of freedom and the resulting trajectories constitute special cases of periodic orbits of the system. We will call them the three principal families. Each of them starts and ends at some of the 14 stationary points of Fig. 1. Physically, as one of the shells is unoccupied, the resulting periodic motion corresponds to simple SU(2) trajectories.

As an example, let us discuss the family $I_2=0$. Then the Hamiltonian reduces to

$$\mathcal{H}(I_1,\theta_1)=-1+I_1+\chi(1-I_1)I_1\cos(2\theta_1) \ . \tag{3.5}$$

which is a one-dimensional stationary Hamiltonian corresponding to the SU(2) Lipkin model.[19]

Figure 3 shows the trajectories at various energies of (3.5) with $\chi=10$ in the (I_1-θ_1) plane (polar coordinates). The family starts at $E=-3.025$ with a two-degenerate stationary point at $\theta_1=\pi/2$ and $3\pi/2$; these stationary points correspond to point A of Fig. 1 (the absolute minimum of the system). As the energy increases, there is a first saddle point (point H of Fig. 1) at $E=-1$ ($I_1=0$) where the two degenerate trajectories coalesce. A second saddle point (I) occurs at $E=0$ ($I_1=1$). Above this energy the solutions appear again in degenerate pairs but now circling around the stationary points at $\theta_1=0$ and π, which correspond to point K ($E=2.025$) of Fig. 1. Since the family starts at a stable point its Lyapunov exponent for low energies is imaginary. At $E\simeq-2.010$ it vanishes and remains real until the end of the family ($E=2.025$), indicating the instability of the family in this energy range.

As a summary of this section we want to emphasize the differences and similarities that this model has with respect to other nonintegrable Hamiltonians with two freedoms that are currently being investigated in connection with soft quantum chaotic systems. First the phase space is compact, leading to an exact quantum description in terms of finite Hermitian matrices, without the need for truncation. Second, the classical limit is obtained as $N\to\infty$. Third, the Hamiltonian cannot be expressed as kinetic plus potential energy. Once these differences have been understood the model can be used for numerical and analytical purposes in exactly the same way as any of the models related to the more usual Weyl group.

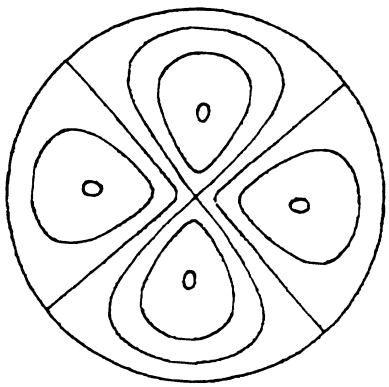

FIG. 3. A family of periodic orbits of the system corresponding to the $I_2=0$ case.

IV. EIGENFUNCTIONS AND CLASSICAL TRAJECTORIES

We are now concerned with the problem of the correspondence between classical trajectories and eigenfunctions.

For that purpose, we have computed the eigenfunctions by diagonalizing the SU(3) Hamiltonian for $\chi=10$ in the (+,+) multiplet, and we have chosen $N=80$ as the number of particles. According to Table I, this results in matrices of dimension 861. The lowest state in energy of the system is then labeled by $|1\rangle$ ($E=-3.0312$), while the upper one by $|861\rangle$ ($E=3.4580$).

The phase-space representation of these eigenfunctions was obtained using the methods of Ref. 13 to calculate the generalized Husimi distributions in action-angle variables as

$$\mathcal{W}_\psi(I,\theta)=\frac{|\langle I\theta|\psi\rangle|^2}{\langle I\theta|I\theta\rangle} \ , \tag{4.1}$$

where $|I\theta\rangle$ is the SU(3) coherent state (2.7) expressed in terms of the action-angle variables (2.8) and ψ is an eigenstate of the system. It provides a smoothed positive definite distribution representing the eigenstate in the four-dimensional phase space labeled by the variables (I,θ). This distribution can be conveniently studied by taking projections and Poincaré sections just as for any classical distribution (see Ref. 13).

A. Association of classical trajectories to eigenfunctions

In order to associate some classical orbits to a given eigenstate, we proceed as follows: we locate the maximum of the four-dimensional phase-space distribution and propagate a classical trajectory from it as an initial condition. The quantum distribution and this classical orbit (that we will call the *dominant trajectory*) can then be compared through their projections and sections; this trajectory will not of course necessarily explain all the features of the eigenfunction.

To identify other classical structures, this procedure can be repeated with other relative maxima of the distribution which are not accounted for by the dominant trajectory. The final result is an association between a single eigenfunction and some classical trajectories. These trajectories can then be said to account for the main features of the eigenfunction.

There is, however, at least one characteristic of the semiclassical limit that compromises the validity and simplicity of this association: the $\hbar$ dependence of the classical phase-space structure detected from the quantum point of view. On the one hand, because quantum mechanically we suppress the infinitely fine complexity of classical phase space through the finite $(2\pi\hbar)^g$ resolution

(g is the number of degrees of freedom), the quantal phase space is *simpler*. But, on the other hand, this finite resolution also implies an $\hbar$ dependence of the existent classical structures. As an example, we mention the fact that quantum mechanically we can detect as a full barrier a classically partial barrier (as a cantorus).[20] In that case, the eigenfunction will be localized by the presence of the cantorus, while the classical trajectory will spread over the entire chaotic region (the classical partial barrier can act as a full barrier from the quantum point of view). We will illustrate this effect in Sec. IV B.

B. Numerical results

We now present the projections and Poincaré sections for some eigenfunctions of the SU(3) model for $\chi=10$, and try to understand their structure in terms of classical orbits.

In all the figures, we have plotted in an $(I_1\text{-}I_2)$ plane the projection of the Husimi distribution $\mathcal{W}_\psi(I,\theta)$ for the quantum pictures [i.e., $\int d\theta_1\, d\theta_2 \mathcal{W}_\psi(I,\theta)$] and the projection of the classical dominant trajectory for the classical pictures. Because of Eq. (2.15) these kind of plots have a triangular shape. In both cases, the associated circle placed on the right of the triangle shows a Poincaré section in polar variables. The I plane employed for that section has been indicated by two small tick marks in the corresponding triangle; for Figs. 4 and 5 the canonical angle conjugate to that plane was fixed by the energy of the quantum state, while in Figs. 7 and 9 it was simply integrated (i.e., projected). For the quantum distributions we have mainly used contour plots, with the upper 95–100% of the projection or section painted in full black and the lower contour line placed at 10% of the maximum.

As an example, let us explain in more detail the first state of Fig. 4, that is $|861\rangle$; other figures are similar. There we have plotted on the triangle the projection on the $(I_1\text{-}I_2)$ plane of the phase-space distribution calculat-

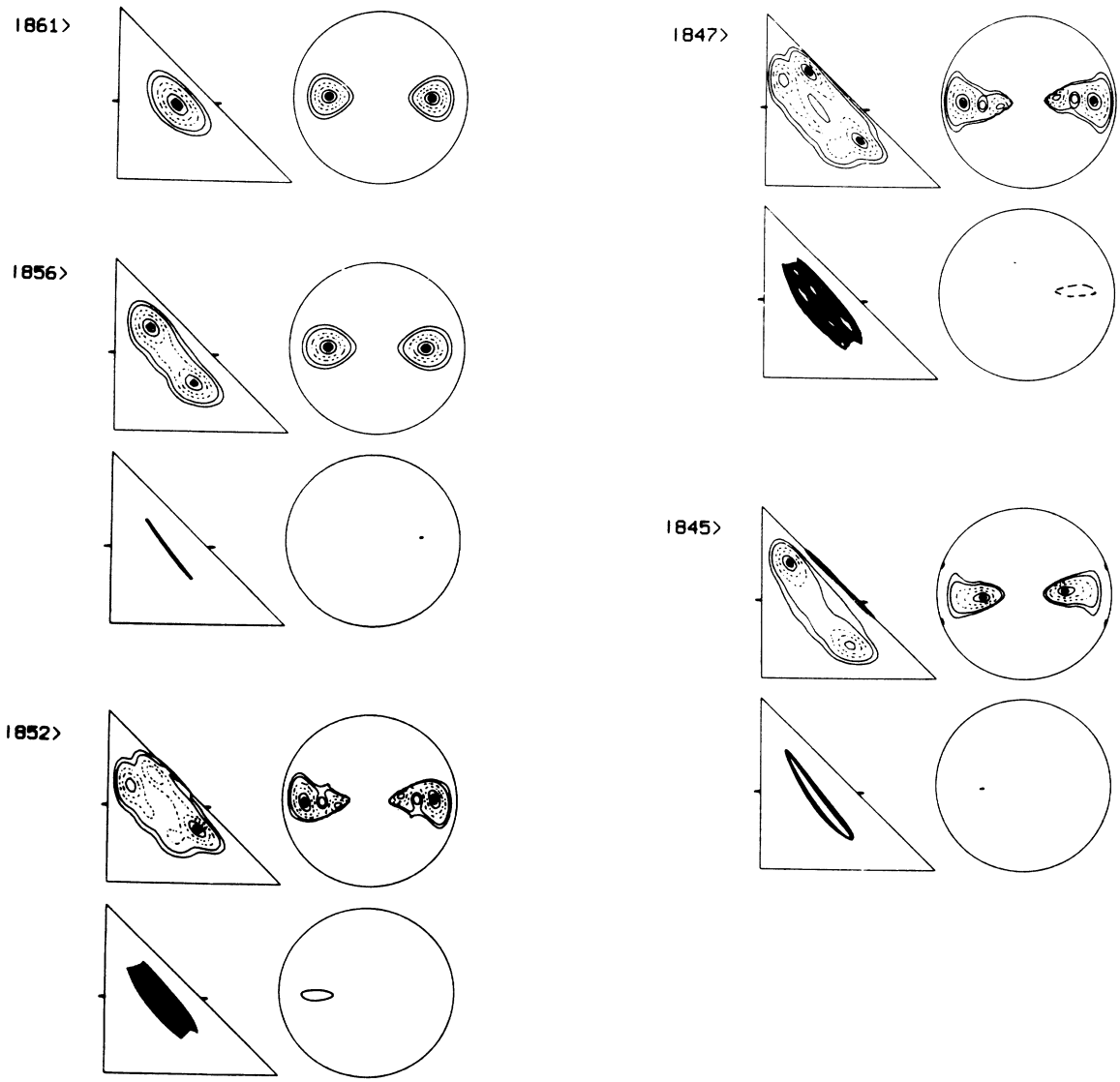

FIG. 4. Projections and Poincaré sections of five eigenfunctions located in the neighborhood of the stable stationary point N (maximum of the system for $\chi=10$). Below each of the eigenfunctions, except for the first one $|861\rangle$, we have plotted the projection and Poincaré section of the associated dominant trajectory. Compare these to Fig. 2. See text for more details.

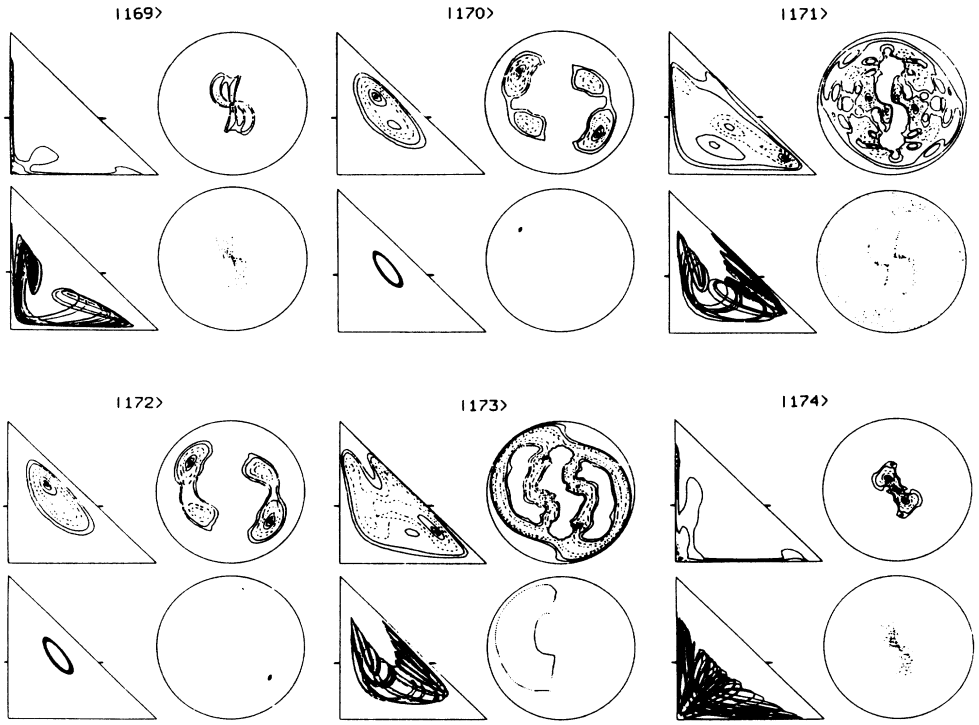

FIG. 5. A sequence of eigenfunctions and their corresponding dominant trajectory for a region of phase space with mixed structure, as is shown in part (a) of Fig. 6.

ed for the state $|861\rangle$. The quantum Poincaré section has been done through the plane $I_2=0.45$, as indicated by the small ticks in the triangle, while the conjugate angle θ_2 was calculated in each point (I_1,θ_1) using Eq. (2.9) for the energy of the eigenstate. When I_2 is fixed in 0.45, the allowed range for I_1 is $0\leq I_2\leq 0.55$ [cf. (2.15)]. What is shown on the right of the triangle is the Poincaré section for the $I_2=0.45$ plane in polar coordinates, where I_1 is the radius and varies from 0 (center of the disk) to 0.55 (edge of the disk) and θ_1 is the angle.

Let us now then show some eigenfunctions associated with the regular regions surrounding a stable stationary point. Figure 4 displays five eigenfunctions lying (in energy) close to the upper stable stationary point (point N of Fig. 1) and whose dominant trajectory is a torus. The first state of the figure is $|861\rangle$, the maximum of the system. This eigenfunction is the first state of the well associated to the classical stable stationary point; the location of this latter point coincides with the full black painted regions of the figure (i.e., the maximum of the distribution is located at the classical stable stationary point). For the remaining four eigenfunctions of the figure, we have plotted in a separate picture below the eigenfunction the classical dominant trajectory.

As was explained in Sec. III, the nearest unstable point to N is point M, whose energy is $E=3.025$. The states $|856\rangle$ and $|852\rangle$ ($E=3.1568$ and $E=3.0357$, respectively) possess an energy lying between these two stationary points. In this energy range, the phase-space structure was shown in Fig. 2(a) ($E=3.1568$). Comparing the dominant trajectories obtained for these two eigenfunctions with Fig. 2(a), we see that the state $|856\rangle$ is dominated by an invariant torus lying very close to the central stable periodic orbit, while the state $|852\rangle$ corresponds to an original parent torus which circles around this periodic orbit. The appearance of two tori in the quantum plot, as opposed to only one in the classical counterpart, is a tunneling effect between tori associated with a symmetry of the Hamiltonian; a classical orbit related by parity also exists.

The states $|847\rangle$ and $|845\rangle$ ($E=2.8946$ and 2.8741, respectively) possess an energy below the unstable stationary point M, and in this case their dominant trajectories must be compared with the phase-space structure of Fig. 2(b). The dominant trajectory of $|847\rangle$ is similar to the $|852\rangle$, but now we have obtained a resonant torus; the state $|845\rangle$ is another state associated with the central periodic orbit. While all the states from $|861\rangle$ to $|852\rangle$ are concentrated on invariant tori, the difference now is that at the energy of states $|847\rangle$ and $|845\rangle$ most tori have been destroyed, and these states coexist, at similar energies, with states lying in the chaotic regions of phase space; these latter states present, however, strong scars in the $I_1+I_2=1$ family of periodic orbits that exists for energies below M (see below).

As is clear from the comparison of the quantum and classical projections and sections, the dominant classical trajectory obtained for the state $|845\rangle$ does not account for all the structures observed in the eigenfunction. In its projection we can see an additional structure located in the $I_1+I_2=1$ axis, whose counterpart in the Poincaré section are four small marks in the circle. The second

classical object besides the dominant trajectory is very easy to identify, since we know from Sec. III that in the plane $I_1+I_2=1$ we have a family of periodic orbits, that starts and ends in the stationary points D and M of Fig. 1, respectively. At the energy of this eigenfunction, this orbit is unstable. We can therefore say that this eigenfunction is "made" of two different classical invariant sets in terms of which we interpret the quantum distribution: a stable periodic orbit (the dominant one, in fact a torus lying very close to the periodic orbit) and an unstable periodic orbit. Other eigenfunctions, combining, for example, two stable trajectories separated by chaotic regions have also been found. The intriguing facts concerning this phenomenon are why these classical objects are combined in a given eigenfunction and how these two (or several) objects are coupled. We do not have a theory for such behavior but some steps towards its understanding were made in Ref. 21.

In order to illustate now the behavior of eigenfunctions in regions of phase space where the system has a mixed structure (i.e., where the volume corresponding to chaotic and regular regions are of the same magnitude), we plot in Fig. 5 a sequence of six consecutive eigenstates close to an energy for which the underlying classical phase-space structure is shown in Fig. 6(a). The available phase space for the same section and energy of part (a) of Fig. 6 is shown in Fig. 6(b). The energy we have used is $E=-1.3770$ and corresponds to the energy of the state $|172\rangle$ of Fig. 5. The dispersion in energy of the group of six states is $\Delta E=0.02$ and we assume that the phase-space structure does not change appreciably in that energy range; we will compare all the dominant trajectories of Fig. 5 with Fig. 6(a) [note how joining up together all the dominant trajectories of Fig. 5 we get a picture similar to Fig. 6(a)].

The eigenfunctions $|170\rangle$, $|172\rangle$, and $|173\rangle$ have their support on regular invariant classical sets, as is clear from the comparison of the classical and quantum plots. States $|170\rangle$ and $|172\rangle$ are very close to a stable periodic orbit, while $|173\rangle$ is related to a torus located near the more chaotic regions of phase space. In the eigenfunctions, a tunneling effect mixes the classical tori related by symmetry, which are not shown in the classical Poincaré sections.

Conversely, the eigenstates $|169\rangle$, $|171\rangle$, and $|174\rangle$ lie on chaotic regions of phase space. The first and the last of them have very similar dominant orbits. However, and in spite of being localized in the same region of phase space, the structure of the quantum Poincaré sections of these eigenfunctions is very different and far from being a uniform distribution in the chaotic region. An interpretation of these eigenfunctions in terms of homoclinic (and heteroclinic) structures belonging to this chaotic region is out of our scope, but remains a very important problem.[21,11]

A very different chaotic dominant trajectory has been obtained for the eigenfunctions $|171\rangle$. The associated chaotic domain is (up to the times of propagation used) disconnected from the remaining chaotic region, presumably due to the presence of a cantorus. However, the quantum section presents a much more complicated structure than the associated dominant trajectory, with an important probability in the regular region close to the stable periodic orbit related with the eigenfunctions $|170\rangle$ and $|172\rangle$.

Other eigenfunctions belonging to the most chaotic regions of phase space ($-1\leq E\leq 1$) have an ergodic-type behavior: they spread over most the energy shell. In Fig. 7 we plot one of these eigenstates, which has $E=-0.106\,25$, using now scattered dots instead of contour lines for the quantum pictures. The classical dominant trajectory is shown below the eigenfunction, as in previous figures. The comparison of the quantum and classical projections and sections shows that the chaotic trajectory accounts for the main features of the Husimi distribution. In order to test the ergodicity of the eigenfunction and classical trajectory, in Fig. 8 we have plotted the accessible region in the section allowed by energy conservation. Clearly the eigenfunction occupies most of the available phase space. However, there is a small nonoccupied region close to the origin in the quantum and classical Poincaré sections. Numerical experiments indicate that this localization is due to a partial barrier (cantorus) that limits the spreading of the eigenstate over the entire energy shell. In fact, if we follow the classical trajectory of Fig. 7 for longer times, the motion finally

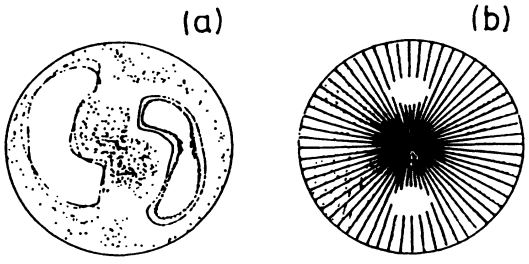

FIG. 6. (a) The structure of phase space associated to the eigenfunctions of Fig. 5. Compare the dominant trajectories of Fig. 5 with this figure. (b) Classical phase space available in the Poincaré sections of Fig. 5 and (a).

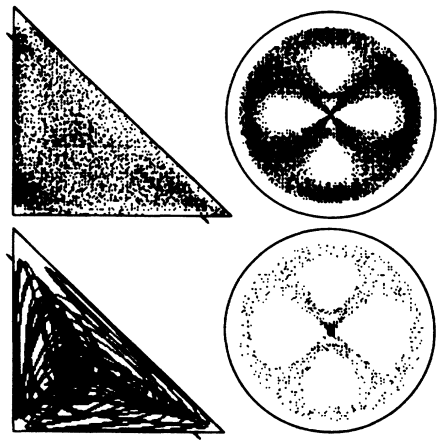

FIG. 7. An eigenfunction having $E=-0.106\,25$ and that spreads over most of the available phase space at that energy (compare with Fig. 8). Its localization is due to the presence of a cantorus.

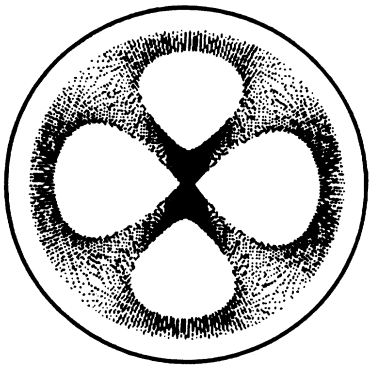

FIG. 8. Phase space available for the energy of the eigenfunction of Fig. 7 and in the same Poincaré section.

enters the nonoccupied region.

We have also found sets of eigenfunctions whose classical support is a (stable or unstable) family of periodic orbits. Simple examples are eigenfunctions related to the three principal families of periodic orbits reported in Sec. III, and for which we have found all members of the quantized one-dimensional corresponding problem. In Fig. 9 we show some of the members of the $I_2=0$ family of eigenstates (using again scattered dots instead of contour plots). They are all characterized by a strong concentration on the $I_2=0$ plane, as is apparent from the projections of the eigenfunctions in the I_1-I_2 plane. The Poincaré sections of these states must be compared with the classical periodic family shown in Fig. 3 [cf. (3.5)]. The state $|1\rangle$ is concentrated near the stable stationary point A at $\theta_1=\pi/2$ and $3\pi/2$, where the classical family starts. As the energy increases, we obtain eigenfunctions associated with all the different types of trajectories of the family, to finally end in the state $|784\rangle$ associated to the unstable stationary point K at $\theta=0$ and $\pi/2$. The first

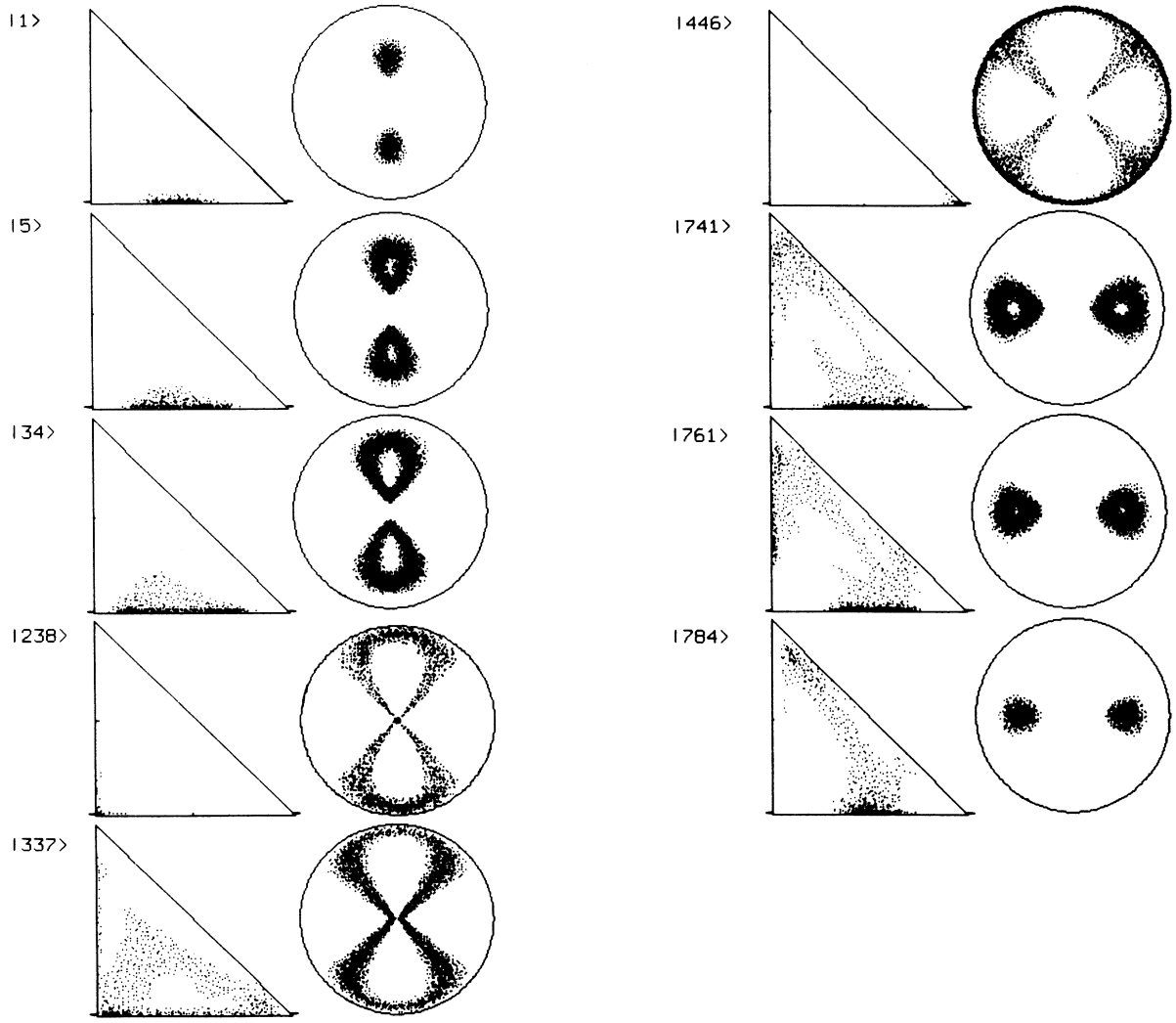

FIG. 9. Some eigenfunctions associated with the classical family of periodic orbits lying in the plane $I_2=0$. The projections are characterized by a strong probability in that plane while the quantum sections must be compared with the classical trajectories shown in Fig. 3.

three states of Fig. 9 lie in the stable energy range of the classical family, while the remaining states are in the unstable range. The instability of the family is reflected in the spreading of the eigengfunctions from the $I_2=0$ axis (compare the projections of states $|1\rangle$ and $|784\rangle$).

The states $|238\rangle$ and $|446\rangle$ are associated with the two saddle points of the family, at $E=-1$ ($I_1=0$) and $E=0$ ($I_1=1$). The strong concentration of these states on an unstable stationary point is remarkable.

Other eigenstates associated with more complicated families of periodic trajectories were also observed. The existence of this type of eigenfunction strongly concentrated on unstable periodic orbits was also observed by Heller[8] in the Bunimovich stadium and by Delande and Gay[22] in the hydrogen atom in a constant magnetic field. Recently a theory of such scars has been developed.[23–25]

V. CONCLUSION

The SU(3) model thus possesses a very complicated classical phase-space structure that we have analyzed in terms of its stationary points and locating its regular and irregular regions. Some simple families of periodic orbits were studied analytically.

Our results for the structure of the Husimi distribution of the eigenstates of a system whose classical phase space is mixed indicate that most eigenfunctions are peaked in one classical invariant set, at least to our precision of 10% of its maximum. These are families of periodic orbits (stable or unstable), tori, or chaotic regions of phase space. In the latter case, some of the eigenfunctions are far from being "uniform" over the chaotic set, but present some structure that probably reflects the influence of unstable periodic orbits. In many cases, the spreading of these eigenstates over the entire accessible chaotic region is also restricted by the presence of cantori.

We must emphasize the coexistence of regular and irregular classical structures that exists at a given energy in the model, a fact that leads in turn to the coexistence of regular and irregular states located in the corresponding regions of phase space. Although the SU(3) model is a very schematic approximation to real nuclei, experimental results indicate that this coexistence actually happens up to very high excited states in the case of ^{152}Dy, where the presence of regular prolate-shaped states immersed in an irregular sequence of levels was detected up to spin $60\hbar$.[26]

However, we have found that the structure of some eigenfunctions cannot be explained in terms of only one classical invariant set. This raises the picture of an eigenfunction as made up from combinations of several classical objects that can be stable or unstable, coupled in a way that we essentially ignored. This conclusion breaks the simple classification scheme of eigenfunctions of such systems into regular and irregular states, due to Percival.[27] Although it seems to be a good approximation for most eigenstates since only one classical trajectory accounts for the main features of its structure, the general scheme emerging from our studies is more complicated, with eigenfunctions combining regular and irregular structures.

ACKNOWLEDGMENTS

We would like to thank M. Baranger for many stimulating and fruitful discussions and to O. Bohigas for his helpful remarks. Division de Physique Théorique is Unité de recherche des Universités de Paris XI et Paris VI associeé au Centre National de Recherche Scientifique (CNRS).

*Present address.

[1]K. Husimi, Proc. Phys. Math. Soc. Jpn. **22**, 264 (1940).

[2]K. Takahashi, J. Phys. Soc. Jpn. **55**, 762 (1986).

[3]J. Kurchan, P. Leboeuf, and M. Saraceno, Phys. Rev. A **40**, 6800 (1989).

[4]M. V. Berry, Phil. Trans. R. Soc. London **287**, 237 (1977).

[5]M. V. Berry, in Proceedings of Les Houches Summer School on Chaos and Quantum Physics, 1989, edited by M. J. Giannoni, A. Voros, and J. Zinn-Justin (North-Holland, Amsterdam, in press).

[6]A. Schnirelman, Usp. Mat. Nank. **29**, 181 (1974).

[7]Y. Colin de Verdière, Commun. Math. Phys. **102**, 497 (1985).

[8]E. J. Heller, Phys. Rev. Lett. **53**, 1515 (1984).

[9]P. W. O'Connor and E. J. Heller, Phys. Rev. Lett. **61**, 2288 (1988).

[10]N. L. Balazs and A. Voros, Ann. Phys. (N.Y.) **190**, 1 (1989).

[11]M. Saraceno, Ann. Phys. (N.Y.) (to be published).

[12]Moreover (Ref. 20), quantum mechanically a cantorus can be "detected" as a full barrier (i.e., a torus) and, as a consequence, only a portion of a chaotic region can constitute, from the quantum point of view, an invariant set.

[13]P. Leboeuf and M. Saraceno, J. Phys. A: Math. Gen. **23**, 1 (1990).

[14]S. Y. Li, A. Klein, and R. M. Dreizler, J. Math. Phys. **11**, 975 (1970).

[15]E. Moya de Guerra and F. Villars, Nucl. Phys. **A298**, 109 (1978).

[16]R. D. Williams and S. E. Koonin, Nucl. Phys. **A391**, 72 (1982).

[17]D. C. Meredith, S. E. Koonin, and M. R. Zirnbauer, Phys. Rev. A **37**, 3499 (1988).

[18]M. Baranger and K. T. R. Davies, Ann. Phys. **177**, 330 (1987); M. A. M. de Aguiar, C. P. Malta, M. Baranger, and K. T. R. Davies, *ibid.* **180**, 167 (1987).

[19]H. J. Lipkin, M. Meshkov, and A. J. Glick, Nucl. Phys. **62**, 188 (1965).

[20]R. S. Mackay, J. D. Meiss, and I. C. Percival, Physica **13D**, 55 (1984); D. Bensimon and L. P. Kadanoff, *ibid.* **13D**, 82 (1984).

[21]Am Ozorio de Almeida, Nonlinearity **2**, 519 (1989).

[22]D. Delande and J. C. Gay, Phys. Rev. Lett. **59**, 1809 (1987).

[23]E. J. Heller, in *Quantum Chaos and Statistical Nuclear Physics,* Vol. 263 of *Springer Lecture Notes in Physics,* edited by T. H. Seligman and H. Nishioka (Springer, New York, 1985).

[24]E. B. Bogomolny, Physica **D31**, 169 (1988).

[25]M. V. Berry, Proc. R. Soc. London Ser. A **423**, 219 (1989).

[26]B. M. Nyakó *et al.*, Phys. Rev. Lett. **56**, 2680 (1986); ;P. J. Twin *et al.*, *ibid.* **57**, 811 (1986).

[27]I. C. Percival, in *Stochastic Behavior in Classical and Quantum Hamiltonian Systems,* Vol. 93 of *Springer Lecture Notes in Physics,* edited by G. Casati and J. Ford (Springer, Berlin, 1979).